Nanocrystalline Y_2O_3:Eu Phosphors Prepared by Alkalide Reduction

Jennifer A. Nelson, Edward L. Brant, and Michael J. Wagner*

Department of Chemistry, The George Washington University, Washington, D.C. 20052

Received July 29, 2002. Revised Manuscript Received November 27, 2002

$(Y_{0.95}Eu_{0.05})_2O_3$ nanoparticles have been synthesized by subambient homogeneous reduction using alkalide solutions and subsequent oxidation. As synthesized, the material consists of free-flowing agglomerates of ill-defined, amorphous, or subnanocrystalline nanoparticles. Samples annealed at 500 °C or greater are crystalline, consisting of agglomerated nanocrystals. As the annealing temperature is raised from 500 to 900 °C, the nanocrystals grow from an average of 10.9 to 14.2 nm, the agglomerates decrease in size, and the surface area increases from 49 to 59 m^2/g. The crystallite size determined by X-ray diffraction line-broadening correlates well with TEM observations, indicating that the particles are individual nanocrystals. The increase in the surface area is consistent with the uncovering of the surfaces of the nanocrystals as a result of the reduction of the size of the agglomerates, counteracting the loss of surface area due to crystallite growth. Annealing at 1000 °C results in growth of the nanocrystals to an average size of 25.1 nm and a decrease in the surface area to 35 m^2/g. Photoluminescence spectra do not show any fluorescence from samples until they have been annealed at 500 °C or higher. Visual inspection found fluorescence from a small fraction of samples annealed at temperatures as low as 200 °C. The photoluminescence intensity of the $^5D_0 \rightarrow {}^7F_2$ transition increases with annealing temperature from 500 to 700 °C, levels-off between 700 and 900 °C, then dramatically increases after annealing at 1000 °C. This trend mirrors that seen for the cell parameter for this cubic system, which decreases from 10.639 to 10.615 Å, larger than the 10.604 Å expected for bulk material. The expanded cell volume may play an important role in the low quantum yields found for these nanocrystalline samples (<8%).

Introduction

Field emission displays (FEDs) can be thought of as the flat panel analogue of the familiar cathode ray tube (CRT). In both cases, the image is produced by phosphors when bombarded by electrons; in a FED, the electrons are produced by an array of field emitting tips. As such, FED technology offers the same excellent display characteristics as the CRT, high brightness and contrast, wide viewing angle, and fast response time.

First generation FEDs employ high excitation voltages (≥5 kV). However, low voltage excitation is required for the development of second generation, low power, portable FEDs.[1] In addition, low voltage FEDs have a number of potential advantages over their high voltage counterparts, including less complexity and, consequently, lower manufacturing costs.[2]

When employing high excitation voltages (≥5 kV), the phosphors used for CRTs can be used in FEDs. However, the efficiency of these phosphors optimized for CRTs drops rapidly as the excitation voltage is lowered below 4 kV. The decreased efficiency is thought to be a result of the reduction in the electron penetration depth as the excitation potential is decreased. For example, the penetration depth for ZnS has been found to drop from 0.5−1.5 μm to 17−27 nm as the voltage is lowered from 10 to 1 kV.[1] Low voltage FEDs require the development of phosphors that are bright and efficient under low energy excitation, are stable at high currents, and have good saturation characteristics.[1,2]

Nanoscale phosphors may have a number of potential advantages over traditional micron-sized phosphors. Nanoscale phosphors offer the possibility of smoother films with higher packing densities, and a larger percentage of cathodoluminescent active material at low excitation voltages due to the reduced electron penetration depth, resulting in an effectively higher luminescent efficiency and resolution than conventional micron-sized phosphors. In addition, quantum confinement in nanocrystalline materials may result in an enhancement of their luminescence.[3−9]

* To whom correspondence should be addressed. Phone: 202-994-6483. Fax: 202-994-2298. E-mail: wagnerm@gwu.edu.

(1) Holloway, P. H.; Trottier, T. A.; Abrams, B.; Kondoleon, C.; Jones, S. L.; Sebastian, J. S.; Thomes, W. J.; Swart, H. *J. Vac. Sci. Technol. B* **1999**, *17*, 758.

(2) Cho, S. H.; Kwon, S. H.; Yoo, J. S.; Oh, C. W.; Lee, J. D.; Hong, K. J.; Kwon, S. J. *J. Electrochem. Soc.* **2000**, *147*, 3143.

(3) Tissue, B. M. *Chem. Mater.* **1998**, *10*, 2837.

(4) Holmes, J. D.; Ziegler, K. J.; Doty, R. C.; Pell, L. E.; Johnston, K. P.; Korgel, B. A. *J. Am. Chem. Soc.* **2001**, *123*, 3743.

(5) Bhargava, R. N.; Gallagher, D.; Hong, X.; Nurmikko, A. *Phys. Rev. Lett.* **1994**, *72*, 416.

(6) Goldburt, E. T.; Kulkarni, B.; Bhargave, R. N.; Taylor, J.; Libera, M. *J. Lumin.* **1997**, *72*−*74*, 190.

(7) Wakefield, G.; Keron, H. A.; Dobson, P. J.; Hutchison, J. L. *J. Colloid Interface Sci.* **1999**, *215*, 179.

(8) Sharma, P. K.; Jilavi, M. H.; Nass, R.; Schmidt, H. *J. Lumin.* **1999**, *82*, 187.

10.1021/cm0207853 CCC: $25.00
Published on Web 01/08/2003

Y_2O_3:Eu is a superior red phosphor with a quantum efficiency of nearly 100%.[10] Commercially, it has applications in fluorescent lamps,[10,11] projection televisions,[10,12] and FEDs.[1,13] As an oxide, it is more stable than sulfur-containing phosphors which undergo changes in their surface chemistry when interacting with the electron beam, seriously degrading their cathodoluminescent brightness and releasing gases that can poison the field emitting tips.[1,14]

Studies of nanocrytalline Y_2O_3:Eu have primarily focused on material produced by gas-phase methods,[15−19] however, two reports of their synthesis by solution methods have recently appeared.[8,20] Sharma and coworkers studied the size dependence of the fluorescence intensity of Y_2O_3:Eu made by coprecipitation in the presence of a surface modifier followed by calcination and found a 5-fold enhancement of the emission intensity as the crystallite size was reduced from 6 μm to 10 nm. This result is similar to that seen for Y_2O_3:Tb nanoparticles made by sol−gel techniques, where the luminescence efficiency was found to vary inversely as the square of the particle size.[6] In both cases, the authors suggested that quantum confinement was responsible for the sharp increase in efficiency with decreasing size. More recently, the opposite trend was noted for Y_2O_3:Eu produced by calcination of oxalates made in emulsion liquid membrane systems.[20] To our knowledge, no other studies of the size dependence of the luminescence efficiency of nanocrystalline Y_2O_3:Eu have appeared, although two reports of the effects of host environments, and the efficiency of 5- and 8-nm nanocrystalline samples, were recently published.[17,18] Here, we report the synthesis of nanocrystalline Y_2O_3:Eu by alkalide reduction and the dependence of their photoluminescence on crystallite size.

Alkalides are crystalline ionic salts consisting of crown ether- or cryptand-complexed alkali metal cations charge-balanced by a stoichiometric number of alkali metal anions.[21,22] Alkalides produce alkali metal anions when dissolved in nonreducible solvents. The alkali metal anion is nearly as thermodynamically powerful a reductant as a solvated electron, the most powerful reductant possible in any given solvent, and is capable of simultaneous two-electron transfers. Alkalide reduction of metal salts results in the formation of a colloid of nanoscale (∼2−15 nm diameter) particles. Colloid stability varies from minutes to hours, depending on the metal reduced and the reaction conditions. Following aggregation and removal of the solvent, the byproducts can be washed away, recovering the crown ether and leaving bare metal nanoparticles. Supported as well as bare particles can be produced.[23−26]

Alkalide reduction has been shown capable of producing alloys and compounds by co-reduction of two metals. In addition, the nanoscale metals have been used as precursors in nitride synthesis.[27] We recently reported the synthesis of Y_2O_3 nanocrystals by alkalide reduction and the dependence of the crystallite size and morphology on annealing temperature.[28] Here we extend that study with the synthesis and characterization of nanoparticulate $(Y_{0.95}Eu_{0.05})_2O_3$ phosphor by postsynthesis oxidation of $Y_{0.95}Eu_{0.05}$ alloy nanoparticles during the removal of byproducts.

Experimental Section

Nanoscale yttrium−europium metal alloy was synthesized by homogeneous alkalide reduction according to the following scheme:

$$3\ K^+(15\text{-crown-}5)_2Na^- + 1.9\ YCl_3 + 0.1\ EuCl_3 \xrightarrow[-20\ °C]{THF} 2\ (Y_{0.95}Eu_{0.05})_{nano} + 3\ K^+(15\text{-crown-}5)_2Cl^- + 3\ NaCl$$

The byproducts were removed by washing the product with aerated H_2O at ambient temperature. This process oxidized the alloy to $(Y_{0.95}Eu_{0.05})_2O_3$ without any apparent evolution of gas. The products were separated from the wash by centrifuge (15 500xG).

YCl_3 and $EuCl_3$ (both anhydrous, 99.99%, packed under Argon) were purchased from Aldrich and used without further purification. Crown ether (15-crown-5, 98%) was purchased from Alfa-AESAR, further dried and then purified by vacuum distillation. Tetrahydrofuran (THF, 99.9+% HPLC grade, inhibitor free) was purified by stirring over KNa alloy until a persistent blue solution was obtained. Reaction vessel loading was performed in a N_2 filled drybox (<1 ppm H_2O and O_2) and solvent transfers were accomplished by vacuum techniques (10^{-6} Torr). Annealing of samples in a free-flowing state was done in air in alumina combustion boats in a tube furnace. Further details of the synthesis can be found elsewhere.[23−28]

Electron micrographs were obtained on a JEM-1200EX transmissions electron microscope (TEM) operating at 80 keV. Samples for TEM were dispersed in MeOH by sonication and deposited on Formvar holey film/carbon coated copper grids. Powder X-ray patterns were obtained with a Scintag XDS-2000 diffractometer (Cu Kα radiation, 1.54 Å) equipped with a liquid N_2 cooled solid-state detector. Thermal analysis, differential calorimetric analysis (DSC), and thermogravimetric analysis (TGA) were performed on Perkin-Elmer Pyris DSC-1 and Pyris TGA-1 instruments respectively, under flowing N_2 gas (20 mL/min). Infrared spectra were obtained with a Perkin-Elmer Spectrum RX FT-IR spectrometer. Elemental analysis was

(9) Jungnickel, V.; Henneberger, F. *J. Lumin.* **1996**, *70*, 238.
(10) Blasse, G.; Grabmaier, B. C. *Luminescent Materials*; Springer-Verlag: New York, 1994.
(11) Peters, T. E.; Pappalardo, R. G.; Hunt, R. B. J. Lamp Phosphors. In *Solid State Luminescence*; Katai, A. H., Ed.; Chapman & Hall: London, 1993; p 313.
(12) Blasse, G. Phosphors for other applications. In *Solid State Luminescence*; Katai, A. H., Ed.; Chapman & Hall: London, 1993; p 349.
(13) Goldburt, E. T.; Bolchouchine, V. A.; Levonovitch, B. N.; Sochtine, N. P. *J. Vac. Sci. Technol. B* **1999**, *17*, 765.
(14) Itoh, S.; Toki, H.; Sate, Y.; Morimoto, K.; Kishino, T. *J. Electrochem. Soc.* **1991**, *138*, 1509.
(15) Kottaisamy, M.; Jeyakumar, D.; Jagannathan, R.; Rao, M. M. *Mater. Res. Bull.* **1996**, *31*, 1013.
(16) Konrad, A.; Fries, T.; Gahn, A.; Kummer, F.; Herr, U.; Tidecks, R.; Samwer, K. *J. Appl. Phys.* **1999**, *86*, 3129.
(17) Schmechel, R.; Kennedy, M.; von Seggern, H.; Winkler, H.; Kolbe, M.; Fischer, R. A.; Xaomao, L.; Benker, A.; Winterer, M.; Hahn, H. *J. Appl. Phys.* **2001**, *89*, 1679.
(18) Schmechel, R.; Winkler, H.; Xaomao, L.; Kennedy, M.; Kolbe, M.; Benker, A.; Winterer, M.; Fischer, R. A.; Hahn, H.; von Seggern, H. *Scripta Mater.* **2001**, *44*, 1213.
(19) Williams, D. K.; Bihari, B.; Tissue, B. M.; McHale, J. M. *J. Phys. Chem. B* **1998**, *102*, 916.
(20) Hirai, T.; Hirano, T.; Komasawa, I. *J. Mater. Chem.* **2000**, *10*, 2306.
(21) Wagner, M. J.; Dye, J. L. *Annu. Rev. Mater. Sci.* **1993**, *23*, 223.
(22) Wagner, M. J.; Dye, J. L. Alkalides and Electrides. In *Comprehensive Supramolecular Chemistry*; Lehn, J. M., Gokel, G. W., Eds.; Elsevier: Oxford U.K., 1996; Vol. 1, p 477.
(23) Tsai, K.-L.; Dye, J. L. *J. Am. Chem. Soc.* **1991**, *113*, 1650.
(24) Dye, J. L.; Tsai, K. L. *Farady Discuss.* **1991**, *92*, 45−55.
(25) Tsai, K. L.; Dye, J. L. *Chem. Mater.* **1993**, *5*, 540.
(26) Cowen, J. A.; Tsai, K. L.; Dye, J. L. *J. Appl. Phys.* **1994**, *76*, 6567.
(27) Chen, X. Z.; Dye, J. L.; Eick, H. A.; Elder, S. H.; Tsai, K.-L. *Chem. Mater.* **1997**, *9*, 1172.
(28) Nelson, J. A.; Wagner, M. J. *Chem. Mater.* **2002**, *14*, 915.

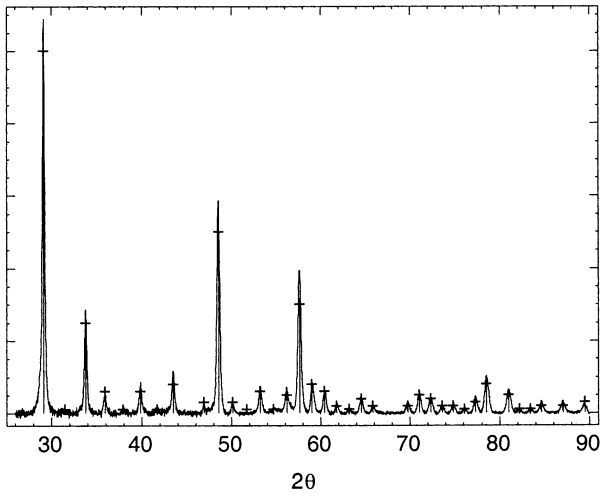

Figure 1. Powder X-ray diffraction pattern of $(Y_{0.95}Eu_{0.05})_2O_3$ nanocrystals following annealing at 1000 °C for 4 h (solid line) and the standard pattern (JCPDS PDF #25-1011, sticks with crosses).

done by flame emission (Perkin-Elmer AAnalyst 100, N_2O/acetylene flame).

Surface area measurements were made on a custom-built (in-house) adsorption apparatus using the BET method with N_2 as the absorption gas and the sample immersed in a liq N_2 bath. The system is based on classical designs and uses two burets with 11 Hg filled bulbs to vary total volume. Pressure was measured with a MKS Instruments 870B capacitance manometer using a 660-B10 power supply/display. The vapor pressure of N_2 at the adsorption temperature (P_o) was measured directly with a Hg manometer. Samples were degassed for 4 h at 400 °C under vacuum (10^{-6} Torr) prior to adsorption measurements. Photoluminescence measurements were performed on a Shimadzu RF-5301PC spectrofluorimeter at ambient temperature. Quantum yields were determined by comparison with the photoluminescence of sodium salicylate excited at 253.7 nm.[29,30]

Results and Discussion

As synthesized at room temperature, the Y:Eu alloy precursor is a black powder. Following washing with aerated H_2O, the Y_2O_3:Eu nanoparticles are in the form of a free-flowing, white powder. The lack of apparent gas evolution during this process is consistent with oxidation of the nanoparticles by dissolved O_2. Powder XRD of the unannealed Y_2O_3:Eu shows only broad features, and selected area electron diffraction (SAD) patterns show only diffuse rings, indicating that the particles are either amorphous or sub-nanocrystalline. Annealing for 4 h at temperatures as high as 400 °C resulted in no significant change in the XRD or SAD patterns. As was seen for Y_2O_3 nanoparticles made by alkalide reduction,[28] annealing at 500 °C or higher resulted in crystallization, observed in X-ray diffractograms that correspond to crystalline cubic $(Y_{0.95}Eu_{0.05})_2O_3$ with no other detectable phases (Figure 1). DSC studies of the heating process fail to reveal any thermal events associated with the crystallization, indicating a second-order thermodynamic process. The product, as synthesized at room temperature, appears to be fully oxidized as no weight gain associated with oxidation is observed by TGA. FT-IR spectra of the products show them to be free of organic byproducts. Elemental analysis confirmed the 5% Eu doping level (5.36 at. %).

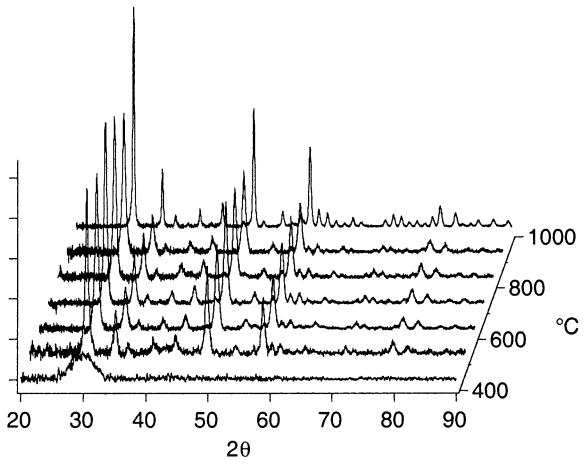

Figure 2. Powder X-ray diffraction patterns of $(Y_{0.95}Eu_{0.05})_2O_3$ nanocrystals annealed for 4 h at the indicated temperature.

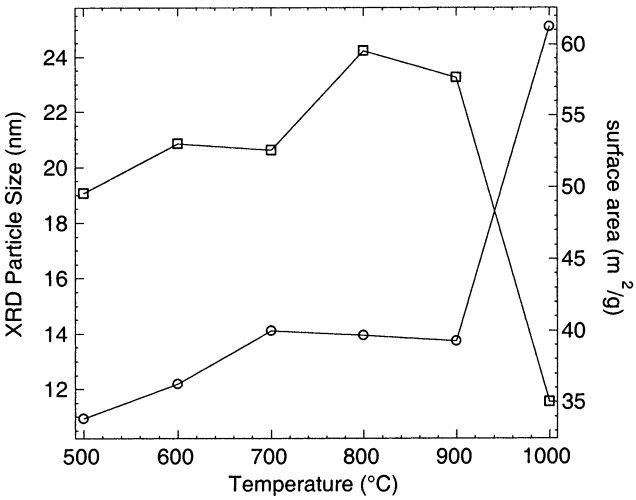

Figure 3. Average crystallite size determined from XRD line broadening (circles) and surface area (squares) plotted as functions of annealing temperature. The lines connecting data points are to guide the eye. Samples were annealed for 4 h at the given temperature.

The XRD peaks sharpened slightly with increasing annealing temperature, indicating some crystallite growth (Figure 2). The crystallite size, as measured from X-ray line broadening, increases from an average of 10.9 to 14.2 nm as the sample annealing temperature is raised from 500 to 700 °C, after which it levels off with little change up to 900 °C (Figure 3). The growth of the crystallites is less pronounced than that seen for undoped Y_2O_3, which increases monotonically from 11.8 to 20.1 nm with increasing annealing temperature from 500 to 900 °C.[28] Much more dramatic growth of the $(Y_{0.95}Eu_{0.05})_2O_3$ occurs upon annealing at 1000 °C, resulting in an average crystallite size of 25.1 nm.

Surface area, measured by the BET method, grows from 49 to 59 m^2/g with increasing annealing temperature from 500 to 900 °C (Figure 3). This behavior is also in contrast to that seen for undoped Y_2O_3, where a smooth decrease in surface area from 84 to 25 m^2/g is observed over the same temperature range.[28] The

(29) Tregellas-Williams, J. *J. Electrochem. Soc.* **1958**, *105*, 173.
(30) Allison, R.; Burns, J.; Tuzzolino, A. J. *J. Opt. Soc.* **1964**, *54*, 747.

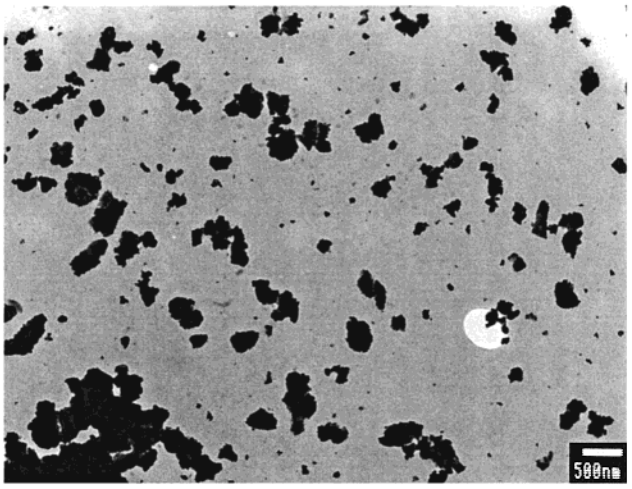

Figure 4. TEM micrograph of $(Y_{0.95}Eu_{0.05})_2O_3$ nanoparticulate agglomerates after annealing at 400 °C for 4 h.

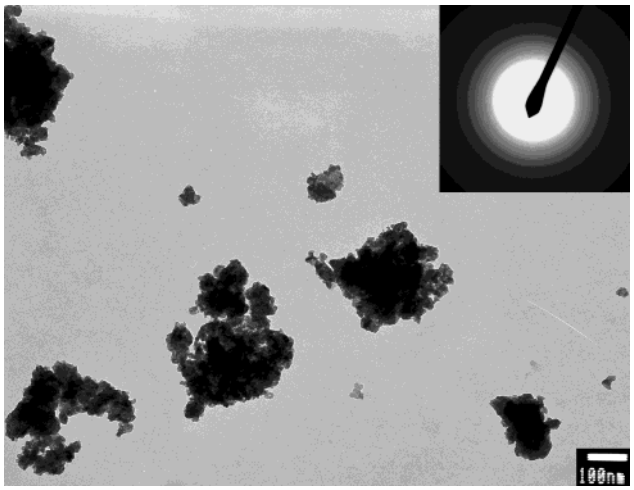

Figure 5. TEM micrograph of $(Y_{0.95}Eu_{0.05})_2O_3$ nanocrystals annealed at 500 °C. Inset is SAD pattern consistent with crystalline $(Y_{0.95}Eu_{0.05})_2O_3$.

surface area of the nanocrystalline $(Y_{0.95}Eu_{0.05})_2O_3$ decreases to 35 m^2/g after annealing at 1000 °C.

TEM observations of the material annealed at or below 400 °C, including the unheated samples, show that they consist of large agglomerates in which it is difficult to distinguish individual nanoparticles (Figure 4). After annealing at 500 °C, the agglomerates are significantly smaller and the nanoparticles of which they are composed are more easily distinguished (Figure 5). The individual particle size correlates well with the XRD crystallite size for all annealing temperatures at or above 500 °C, indicating that the agglomerates are composed of individual nanocrystals. SAD patterns match those expected for crystalline $(Y_{0.95}Eu_{0.05})_2O_3$, becoming sharper as the annealing temperature is increased, in agreement with the observed crystallite growth. The agglomerate size decreases with increasing temperature, and the nanocrystals of which they are composed become more easily distinguished, indicating that they are breaking up as the crystallites grow (Figure 6). It is apparent that the exposure of additional surfaces with the break-up of the agglomerates results in an increase in surface area even though the crystallite size grows or stays constant as the annealing temperatures is raised from 500 to 900 °C. The large

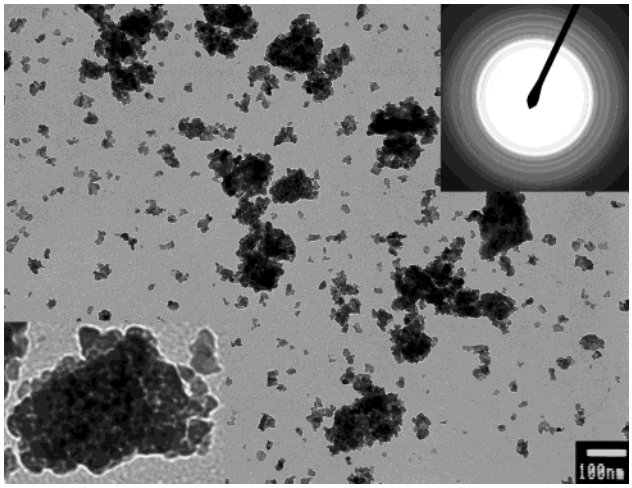

Figure 6. TEM micrograph of $(Y_{0.95}Eu_{0.05})_2O_3$ nanocrystals annealed at 700 °C. Upper right inset is SAD pattern consistent with crystalline $(Y_{0.95}Eu_{0.05})_2O_3$, lower left is a 4× magnified portion of micrograph showing the structure of a cluster.

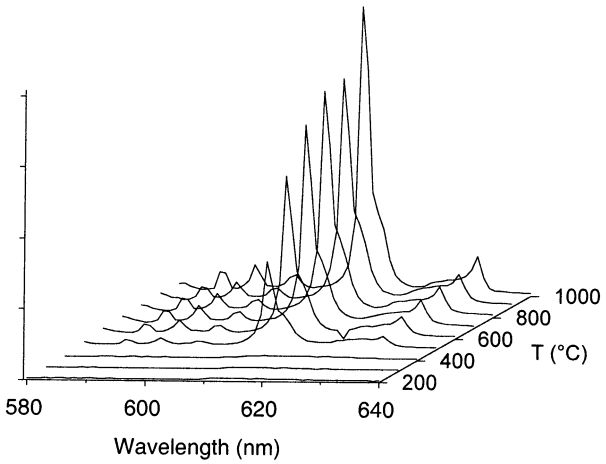

Figure 7. Photoluminescence spectra, excited at 253 nm, of nanoparticulate $(Y_{0.95}Eu_{0.05})_2O_3$ annealed for 4 h at the indicated temperatures.

decrease in the surface area following annealing at 1000 °C is consistent with the dramatic crystallite growth observed by TEM and XRD.

Photoluminescence spectra show little fluorescence from samples that were annealed at 400 °C or lower. For samples annealed at 500 °C or greater, luminescence spectra characteristic of Y_2O_3:Eu are observed. The intensity of the fluorescence increases with increasing annealing temperature (Figure 7), in contrast to the behavior observed by Sharma and co-workers,[8] but in agreement with that observed by Hirai and co-workers.[20] The red-orange luminescence is clearly visible in room light when excited by a standard hand-held laboratory UV source (254 nm, Spectroline model ENF-240C, Spectronics Corporation). Figure 8, taken with a digital camera in a darkened room, shows that a small portion of the material annealed between 200 and 400 °C is fluorescent (visible speckles of orange-red).

Typical photoluminescence excitation spectra, measured for the 611 nm line, are shown in Figure 9. The excitation spectra of samples annealed from 500 °C to 900 °C are identical when corrected for quantum efficiency. They show the expected charge-transfer band that is narrower than that reported for bulk material

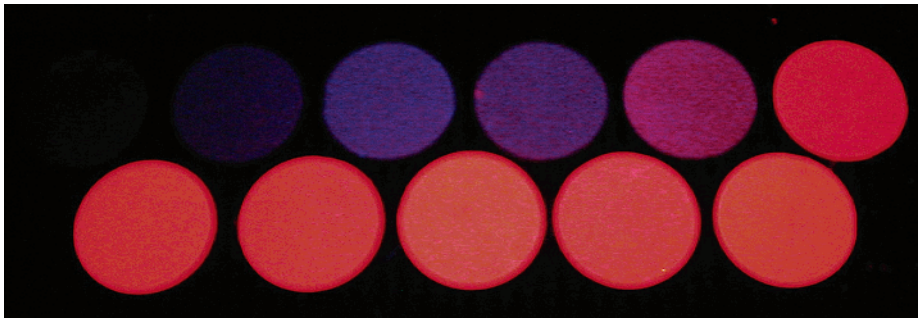

Figure 8. Photograph of luminescencing nanocrystalline $(Y_{0.95}Eu_{0.05})_2O_3$ pellets. The samples are arranged in order of increasing annealing temperature starting from unannealed (upper left, not visible) through 500 °C (upper right), and 600 °C (lower left) through 1000 °C (lower right).

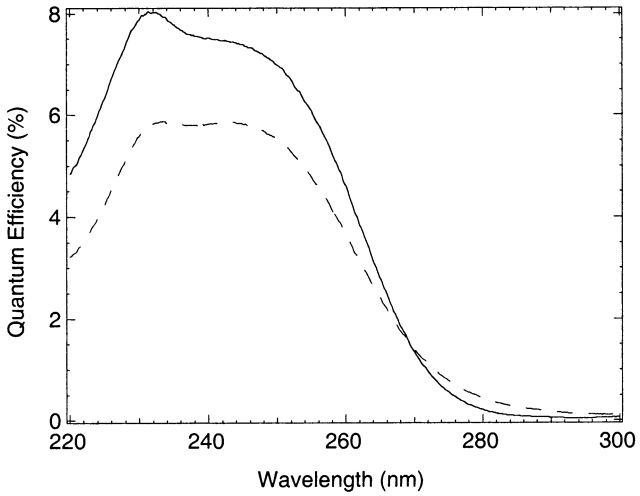

Figure 9. Photoluminescence quantum efficiency of $(Y_{0.95}Eu_{0.05})_2O_3$ nanocrystals annealed at 900 °C (dashed line) and 1000 °C (solid line) plotted as functions of excitation wavelength.

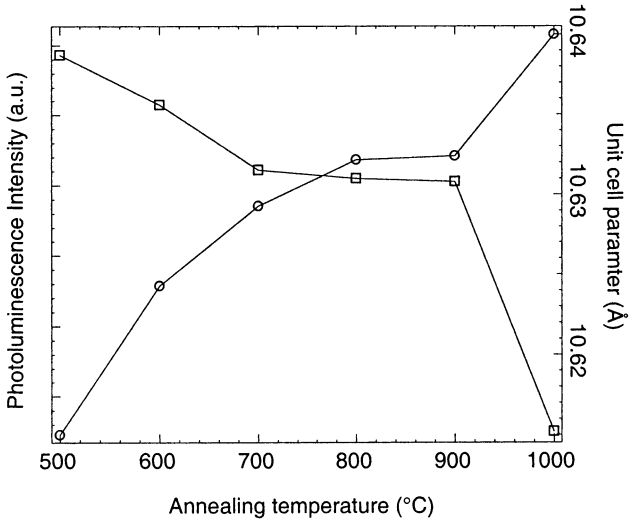

Figure 10. Photoluminescence intensity of the 611 nm $^5D_0 \rightarrow {}^7F_2$ peak (circles) and the cell parameter (squares) plotted as a function of annealing temperature.

but similar to that reported for 8-nm nanocrystals.[18] Annealing at 1000 °C resulted in a narrowing of the excitation spectra and an increase in a narrow feature at ~232 nm. The origin of this feature is uncertain. The general shape of the excitation spectrum suggests that it may be associated with host lattice (exiton) absorption. However, this seems unlikely as it is red-shifted more that 20 nm from that previously seen in bulk and nanocrystalline material.[16−18]

The quantum efficiency of our nanocrystals, even after annealing at 1000 °C, is significantly lower than bulk, but slightly higher than that seen in all other reports of which we are aware.[17,18] In addition, although researchers have found that the quantum efficiency of nanocrystalline Y_2O_3:Eu decreases with extended exposure to ambient atmosphere, we noted no change after 3 months in any of our samples.

The increase in the surface-to-volume ratio consequent to the reduction in crystallite size would seem to offer a straightforward explanation for the lower quantum efficiency we see for nanocrystalline $(Y_{0.95}Eu_{0.05})_2O_3$. As the particle size is reduced, the surface becomes more accessible to the excitation centers, allowing for an increase in nonradiative surface recombination. However, other investigators have found that the lifetime of the $^5D_0 \rightarrow {}^7F_2$ transition is actually longer by a factor of 3 for nanocrystalline Y_2O_3:Eu, rather than shorter as one might expect if surface recombination relaxation is enhanced.[17,18,31] Schmechel and co-workers have offered a qualitative explanation for these seemingly contradictory results that may be equally applicable to the nanocrystals described in this report.[17] Eu^{3+} is located in two crystallographic sites in Y_2O_3: an 8b site with S_6 symmetry and a 24d site with C_2 symmetry. The $^5D_0 \rightarrow {}^7F_2$ transition is electric dipole forbidden in crystal sites that have inversion symmetry, as it is in the free ion. However, as the 24d site does not have inversion symmetry, and mixing of the $4f^{(n-1)}5d$ states by odd components of the crystal field results in a "forced" electric dipole transition responsible for the observed luminescence.[32,33] Schmechel and co-workers suggested that the increased lattice constant they observed in nanocrystalline Y_2O_3 (10.641 vs 10.604 Å in bulk) was responsible for the increased lifetime of the $^5D_0$ state, because "forced" electric dipole transitions are hypersensitive to small changes in the crystal field. It was concluded that the lower quantum yield probably arises from a greatly reduced radiative transition rate, probably due to lattice expansion, and an enhanced nonradiative transition rate, possibly due to increased multiphonon emission mediated by surface adsorbates.

To test the applicability of the conclusions of Schmechel and co-workers to the nanocrystalline material re-

(31) Bihari, B.; Eilers, H.; Tissue, B. M. *J. Lumin.* **1997**, *75*, 1.
(32) Judd, B. R. *Phys. Rev.* **1962**, *127*, 750.
(33) Ofelt, G. S. *J. Chem. Phys.* **1962**, *37*, 511.

ported here, we determined the lattice constants for each of our samples (Figure 10). Samples annealed at 500 °C were found to have a lattice constant of 10.639 Å. The lattice constant decreases as the annealing temperature is increased to 700 °C, then levels until decreasing dramatically to 10.615 Å following annealing at 1000 °C. Also plotted in Figure 10 is the photoluminescence intensity of the $^5D_0 \rightarrow {}^7F_2$ transition which mirrors the behavior of the cell parameter, consistent with what might be expected if the radiative relaxation rate is closely tied to changes in the crystal field brought about by the lattice expansion. It should be noted that the growth of the average crystallite size shows the same trend, thus one should not rule out the possibility that the change in surface-to-volume ratio, and thus the accessibility of surface recombination states, may play an important role. In addition, annealing may result in a reduction in bulk and surface defects, which presumably would decrease the nonradiative relaxation rate.

Conclusions

Nanoparticulate $(Y_{0.95}Eu_{0.05})_2O_3$ can be readily synthesized by alkalide reduction. Altering the Eu^{3+} content should be possible by adjusting the reaction stoichiometry. As synthesized, the material is amorphous or subnanocrystalline and strongly agglomerated. Annealing the nanoparticles at 500 °C or higher results in nanocrystalline material that displays photoluminescence characteristic of Eu^{3+}-doped yttria. As the annealing temperature is raised from 500 to 1000 °C, the nanocrystals grow, the agglomerates break up, and the photoluminescence intensity increases. However, even after annealing at 1000 °C, the quantum yield is low, less than 8%. The cell parameters, which are larger than expected for bulk, decrease as the annealing temperature is raised, mirroring the behavior of the luminescence, suggesting a correlation with the low quantum yields observed.

Acknowledgment. We thank Dr. Robin Rufner and the George Washington University Center for Microscopy and Image Analysis for assistance and use of the TEM imaging facilities. In addition, we thank Professor Richard G. Weiss and Dr. Chuping Luo of the Department of Chemistry at Georgetown University for assistance with preliminary photoluminescence measurements. Finally, we thank the National Science Foundation for financial support (DMR-9876164).

CM0207853